

This work was written as part of one of the author's official duties as an Employee of the United States Government and is therefore a work of the United States Government. In accordance with 17 U.S.C. 105, no copyright protection is available for such works under U.S. Law.

Public Domain Mark 1.0

<https://creativecommons.org/publicdomain/mark/1.0/>

Access to this work was provided by the University of Maryland, Baltimore County (UMBC) ScholarWorks@UMBC digital repository on the Maryland Shared Open Access (MD-SOAR) platform.

Please provide feedback

Please support the ScholarWorks@UMBC repository by emailing scholarworks-group@umbc.edu and telling us what having access to this work means to you and why it's important to you. Thank you.



COMMIT in 7-SEAS/BASELInE: Operation of and Observations from a Novel, Mobile Laboratory for Measuring *In-Situ* Properties of Aerosols and Gases

Peter Pantina^{1,2*}, Si-Chee Tsay², Ta-Chih Hsiao³, Adrian M. Loftus^{2,4}, Ferret Kuo⁵, Chang-Feng Ou-Yang⁵, Andrew M. Sayer^{2,6}, Sheng-Hsiang Wang⁵, Neng-Huei Lin⁵, N. Christina Hsu², Serm Janjai⁷, Somporn Chantara⁸, Anh X. Nguyen⁹

¹ Science Systems and Applications, Inc., Lanham, Maryland, USA

² NASA Goddard Space Flight Center, Greenbelt, Maryland, USA

³ Graduate Institute of Environmental Engineering, National Central University, Chung-Li 32001, Taiwan

⁴ ESSIC, University of Maryland, College Park, Maryland, USA

⁵ Department of Atmospheric Sciences, National Central University, Chung-Li 32001, Taiwan

⁶ GESTAR/USRA, Columbia, Maryland, USA

⁷ Silpakorn University, Nakhon Pathom, Thailand

⁸ Faculty of Science, Chiang Mai University, Chiang Mai, Thailand

⁹ Vietnam Academy of Science and Technology, Hanoi, Vietnam

ABSTRACT

Trace gases and aerosols (particularly biomass-burning aerosols) have important implications for air quality and climate studies in Southeast Asia (SEA). This paper describes the purpose, operation, and datasets collected from NASA Goddard Space Flight Center's (NASA/GSFC) Chemical, Optical, and Microphysical Measurements of *In-situ* Troposphere (COMMIT) laboratory, a mobile platform designed to measure trace gases and optical/microphysical properties of naturally occurring and anthropogenic aerosols. More importantly, the laboratory houses a specialized humidification system to characterize hygroscopic growth/enhancement, a behavior that affects aerosol properties and cloud-aerosol interactions and is generally underrepresented in the current literature. A summary of the trace gas and optical/microphysical measurements is provided, along with additional detail and analysis of data collected from the hygroscopic system during the 2015 Seven South-East Asian Studies (7-SEAS) field campaign. The results suggest that data from the platform are reliable and will complement future studies of aerosols and air quality in SEA and other regions of interest.

Keywords: Biomass-burning; Aerosol; *In-situ*; 7-SEAS, BASELInE; Air quality; Hygroscopicity.

INTRODUCTION

Aerosols (e.g., dust, soot, black carbon, organic carbon, sea salt) and trace gases such as carbon dioxide (CO₂), carbon monoxide (CO), ozone (O₃), nitric oxide (NO), nitrogen dioxide (NO₂), and sulfur dioxide (SO₂) are of special interest to air quality and climate studies because they play an active role in modulating Earth's radiative forcing (via atmospheric absorption/scattering), long-term climate processes (Booth *et al.*, 2012; Lin *et al.*, 2014), as well as human health and life expectancy (Brook *et al.*, 2010; Brauer *et al.*, 2012). Ground-based measurements provide an *in-situ* source of

aerosol and gas information for direct analysis and for calibration/validation of observations derived from satellite, suborbital, and other *in-situ* or remote sensing platforms.

For Southeast Asia (SEA), aerosol and air quality studies are of particular interest. In past studies, the area around northern Thailand has been described as a major active source for biomass burning (BB), air pollution, and fires in South Asia (Chan *et al.*, 2003; Chantara *et al.*, 2012; Chuessard *et al.*, 2014; Lin *et al.*, 2014; Wang *et al.*, 2015). Gautam *et al.* (2013) used satellite and ground-based radiometric observations over five years to specify the Thailand-Myanmar border region as a BB hotspot during the springtime dry (pre-monsoon) season. BB aerosols are particulates emitted and suspended in the atmosphere as a result of anthropogenic fires started to clear land, cook, or eliminate waste. These aerosols may also be generated by naturally occurring wildfires. Additional studies have demonstrated that BB aerosols generated in SEA undergo long-range transport to

* Corresponding author.

Tel.: +13016146202; Fax: +13016146307

E-mail address: peter.pantina@nasa.gov

the north and east at upper levels and settle in areas as far away as Taiwan, some 2400 kilometers (km) northeast of western Thailand (Chan *et al.*, 2003; Lin *et al.*, 2009; Huang *et al.*, 2013; Yen *et al.*, 2013; Lin *et al.*, 2014). Bell *et al.* (2013) identified regions within the South China Sea, east of Mainland SEA, as an area where the effects of BB aerosols are combined with those of naturally occurring mineral dust and maritime aerosols. Lin *et al.* (2014) used satellite and ground-based observations and simulations to demonstrate that source aerosols generated over SEA had a net negative radiative effect at ground level and at top of the atmosphere, as well as a positive effect in between. In addition, they isolated a zone stretching from southern China to Taiwan where surface shortwave radiation was reduced as a result of these aerosols. Thus it is evident that natural and anthropogenic (particularly BB) aerosols play a major role in SEA air quality.

Aerosol optical/microphysical properties and trace gas concentrations associated with BB have been the subject of several studies on air quality. Trace gases act as strong markers and help to differentiate types and sources of pollution regimes (Chan *et al.*, 2003; Poncanart and Akimoto, 2003; Andreae and Merlet, 2011; Kondo *et al.*, 2011; Tsai *et al.*, 2013; Ou-Yang *et al.*, 2016). The same is true for aerosol spectral single scattering albedo (SSA), the ratio of aerosol scattering to total (absorption plus scattering) extinction, which also affects climate (Eck *et al.*, 1999; Petzold *et al.*, 2013, and references therein). Microphysical properties of aerosols (e.g., particle diameter, particle mass concentration, particle size distribution [PSD]) correlate well with respiratory and cardiovascular health (Kristensson *et al.*, 2013; Lelieveld *et al.*, 2015) but also have implications for cloud-aerosol interaction studies (Lance *et al.* 2006), among others.

Hygroscopic properties remain an important factor in understanding aerosol behavior. Depending on the composition and size of aerosol particles, as well as the relative humidity (RH) of the ambient air, aerosols can absorb water and increase in size as RH increases beyond a certain value, called the deliquescence point. Moistened particles can display different optical properties (Tao *et al.*, 2014), exhibit PSDs shifted toward larger particle diameters (Rissler *et al.*, 2006; Hu *et al.*, 2013), and experience enhanced scattering and radiative effects (Hervo *et al.*, 2014) compared to their dry counterparts. These effects are different for drying particles, since recrystallization does not necessarily occur at the deliquescence point, leading to complicated aerosol hysteresis effects, which were first demonstrated by Orr *et al.* (1958). Englehard *et al.* (2012) concluded that hygroscopic properties also differ and act as a marker between primary and aged aerosols, where primary aerosols that have not been aged by photochemical oxidation show higher hygroscopic growth variability than secondary organic aerosols. Climate models may suffer from not parameterizing these effects (e.g., Khylstov *et al.*, 2005; Bell *et al.*, 2013), and lack of hysteresis data creates a “significant gap” in aerosol studies according to Reid *et al.* (2005). Analysis of hygroscopic growth is therefore a primary interest in many recent aerosol studies and is a main focus of the most recent observations.

Since man-made and naturally occurring aerosols

generated within mainland SEA can travel long distances and affect the radiation budget, climate, and human health along the pathway, the development and deployment of a comprehensive, reliable suite of instruments for measuring hygroscopic, optical, and microphysical properties of aerosols and trace gases will have a positive impact on the understanding of air quality and climate in SEA. It will serve as a platform to increase the temporal resolution of data offered by polar-orbiting satellites, and to intercompare with data products retrieved from geostationary satellites. Over the course of the past ten years, the NASA Goddard Space Flight Center’s (NASA/GSFC) Chemical, Optical, and Microphysical Measurements of *In-situ* Troposphere (COMMIT) ground-based mobile laboratory has participated in field campaigns at various international locations, most recently concentrated in SEA. During each experiment, a broad range of air quality/aerosol instruments operate continuously and archive quality-controlled, high temporal resolution, and calibrated data products.

In this paper, we provide a brief description of the most recent sites to which COMMIT has been deployed. Next we detail facility operations, then provide a brief overview of trace gas and optical/microphysical aerosol measurements, followed by a detailed description of a hygroscopic analysis system as it applies to optical scattering and aerosol PSD measurements. Finally, we summarize results from recent campaigns and conclude with suggestions for future work. The primary intent of this study is therefore to provide a point of reference for COMMIT’s standard operating procedures (SOP) for field campaigns and to highlight a unique method of measuring hygroscopic properties of BB aerosols in SEA. Detailed analyses using the results obtained during campaigns are presented in other papers within this special issue (Tsay *et al.*, 2016 and references therein).

DEPLOYMENT SITES AND OPERATIONS

Deployment Sites

Measurements from the most recent field campaign were collected at the meteorological station in Doi Ang Khang (DAK), Chiang Mai Province, Thailand (19.93°N, 99.05°E, 1518 meters [m] above sea level). This intensive operation period was part of the larger Seven South-East Asian Studies/Biomass-burning Aerosols and Stratocumulus Environment: Lifecycles and Interactions Experiment (7-SEAS/BASELInE) field campaign, which has been ongoing since 2013, and since 2010 as a precursor, the 7-SEAS/Dongsha Experiment (Lin *et al.* 2013). The site is located in the mountainous northwestern terrain of Thailand, around 125 km north of Chiang Mai. Data were collected from February to April 2015, during the peak of the BB source activities in SEA. Prior to the experiment it was assumed that a large portion of the aerosol loading would be generated from local BB activities, which was at least qualitatively confirmed by observation of daily burning events for clearing of forested land and agricultural fields.

Previous 7-SEAS experiments involving the COMMIT mobile laboratory were conducted at the meteorological station in Son La (SL), Vietnam, (21.33°N, 103.90°E, 660 m

above sea level) during Spring 2012 and 2013 (Tsay *et al.*, 2013). Investigations completed here provide continuity in instrument data sets and contribute to the study of the evolution of atmospheric pollutants as they move downstream and age from their source regions. Local anthropogenic BB activities have a strong influence on the region's air quality as well. During 2013, the Aerosol-Cloud-Humidity Interactions Exploring and Validating Enterprise (ACHIEVE) mobile laboratory was deployed downstream of the SL site, and it provided the remote-sensing data detailed in Loftus *et al.* (2016). ACHIEVE's mission is focused on understanding aerosol-cloud interactions, to which COMMIT's aerosol and hygroscopic growth data will provide helpful modeling

constraints.

Facility Operations

In total, over 25 instruments operate simultaneously inside COMMIT. Instrument data streams include aerosol observations at up to 1 Hertz (Hz) temporal resolution. Table 1 provides more information on the individual instruments available with the COMMIT platform. All instruments referenced in this paper will be referred to using the abbreviations listed there.

The system is housed in a 20-foot weatherproof sea container (Seabox, Inc., USA) that can be made fully operational from a packed state in less than one day. All

Table 1. Names (abbreviations), models, specifications (measurement types, ranges, wavelengths, resolutions [Res.]), and manufacturer (Mfr.) for instruments operating inside COMMIT.

	Instrument	Model	Specifications			Mfr.
			Measurement	Range	Res.	
Optical	Cavity-Attenuated Phase Shift Extinction Monitor (PMEx)	Blue, Green, Red	σ_e (10^{-6} m^{-1})	445 nm, 530 nm, and 630 nm	1 sec.	Aerodyne Research, Inc., USA
	Aethalometer (AE31)	AE31	σ_a (10^{-6} m^{-1})	370 nm, 470 nm, 520 nm, 590 nm, 660 nm, 880 nm, and 950 nm	5 min.	Magee Scientific Corp., USA
	Particle Soot/Absorption Photometer (PSAP)	3 λ	σ_a (10^{-6} m^{-1})	470nm, 522nm, and 660nm	1 sec.	Radiance Research, Inc., USA (defunct)
	Nephelometer (NEPH) Wet & Dry	TSI-3563	σ_s (10^{-6} m^{-1})	450 nm, 550 nm, and 650 nm	5 min.	TSI, Inc., USA
Microphysical	Beta Attenuation Monitor (BAM) 2.5 & 10	BAM-1020	PM _{2.5} ($\mu\text{g m}^{-3}$) PM ₁₀ ($\mu\text{g m}^{-3}$)	0–1000 $\mu\text{g m}^{-3}$	60 min.	MetOne Instruments Inc., USA
	Tapered Element Oscillating Microbalance (TEOM)	1400a	PM ₁ ($\mu\text{g m}^{-3}$)	5 $\mu\text{g m}^{-3}$ –several gram m^{-3}	5 min.	Thermo Fisher Scientific Inc., USA
	Aerodynamic Particle Sizer (APS)	TSI-3321	Particle distribution (# cm^{-3})	0.523–19.8 μm	6 min.	TSI, Inc., USA
	Fast Mobility Particle Sizer (FMPS)	TSI-3091	Particle distribution (# cm^{-3})	6.04–523 nm	1 sec.	TSI, Inc., USA
	Scanning Mobility Particle Sizer (SMPS) Wet & Ambient	SMPS (TSI-3936) Classifier (TSI-3080) DMA (TSI-3081) Condensation Particle Counter (TSI-3787)	Particle distribution (# cm^{-3})	16.8–982 nm	6 min.	TSI, Inc., USA
	Cloud Condensation Nuclei (CCN) Counter	CCN-100	Cloud condensation nuclei (# cm^{-3})	0.1%, 0.2%, 0.4%, 0.6%, and 0.8% super saturation	1 sec.	Droplet Measurement Technologies, USA
Gas	Gas Monitors	146C (Calibrator), 41C (CO ₂), 48C (CO), 43C (SO ₂), 49C (O ₃), 42C (NO-NO ₂ -NO _x)	CO ₂ , CO, SO ₂ , O ₃ , NO, NO ₂ , NO _x , and NO _y concentrations (parts per million)		1 min.	Thermo Fisher Scientific Inc., & Air Quality Design, Inc., USA
Ancillary	Weather Transmitter (WXT520)	WXT520	Temp. (°C), pressure (millibar), RH (%), wind speed (m s^{-1}), and rainfall (millimeters)		1 min.	Vaisala, Finland
	Visibility Meter (VIS)	OWI-430	Visibility (km) and temp. (°Celsius)		1 min.	Optical Scientific, Inc., USA

instrument setup, daily operating, maintenance, and calibration routines are well documented in a set of SOPs, which are publically available at <http://www.smartlabs.gsfc.nasa.gov>. For most instruments, ambient air is sampled at 7 m above the laboratory roof and is drawn into a 15-centimeter (cm) diameter metal stack (Fig. 1) via a blower. Air flows through the stack such that the flow across the cross-sectional area of the stack is ten times higher than the flow across the individual sampling ports so that flow is approximately isokinetic. At the base of the main stack, several stainless steel pipes are installed to direct the airflow into various rack-mounted instruments via conductive tubing with minimal bend. Tube diameters and flow pathways were chosen to minimize particle loss and to balance the flow among the different instruments. Beta Attenuation Monitors (BAMs) and a Tapered Element Oscillating Microbalance (TEOM) sample air independently from the main stack via vacuum pumps. Nephelometer (NEPH) flow is reported in the DAK campaign with a $PM_{2.5}$ size-cut for this particular study. However, the cyclone may be replaced/removed if particular/full-range particle sampling is desired.

All instruments, where possible, undergo flow checks,

zero-air (i.e., particle-free air) checks, and intercomparisons before and after the experiment to ensure quality data and consistent operation of the equipment (Table 2). Flows are monitored using a Gillian bubble meter (Sensidyne LP, USA), which was cross-checked with an independently calibrated flow meter during the most recent campaign. Zero-air is generated using a chemical scrubbing method, in which compressed air is passed at ~30 psi through a dehumidifier (Twin Towers Engineering, Inc., USA) and a series of chemical scrubbers containing Purafil (Purafil, Inc., USA), Drierite (W. A. Hammond Drierite Co. Ltd., USA), sodalime, and activated charcoal. This routine has demonstrated effectiveness in past studies (Rutter *et al.*, 2012). All scrubbers are changed before and after each campaign, with more frequent changes to Drierite to ensure dehumidification of the incoming air. For cases where quick, filtered air is required, a fresh high-efficiency particulate arrestance (HEPA) filter is placed in the sampling line.

Data streams are collected and archived using a centralized command and data handling system that provides a virtualized platform and a consistent manner in which to interact with the independent instruments. It offers large

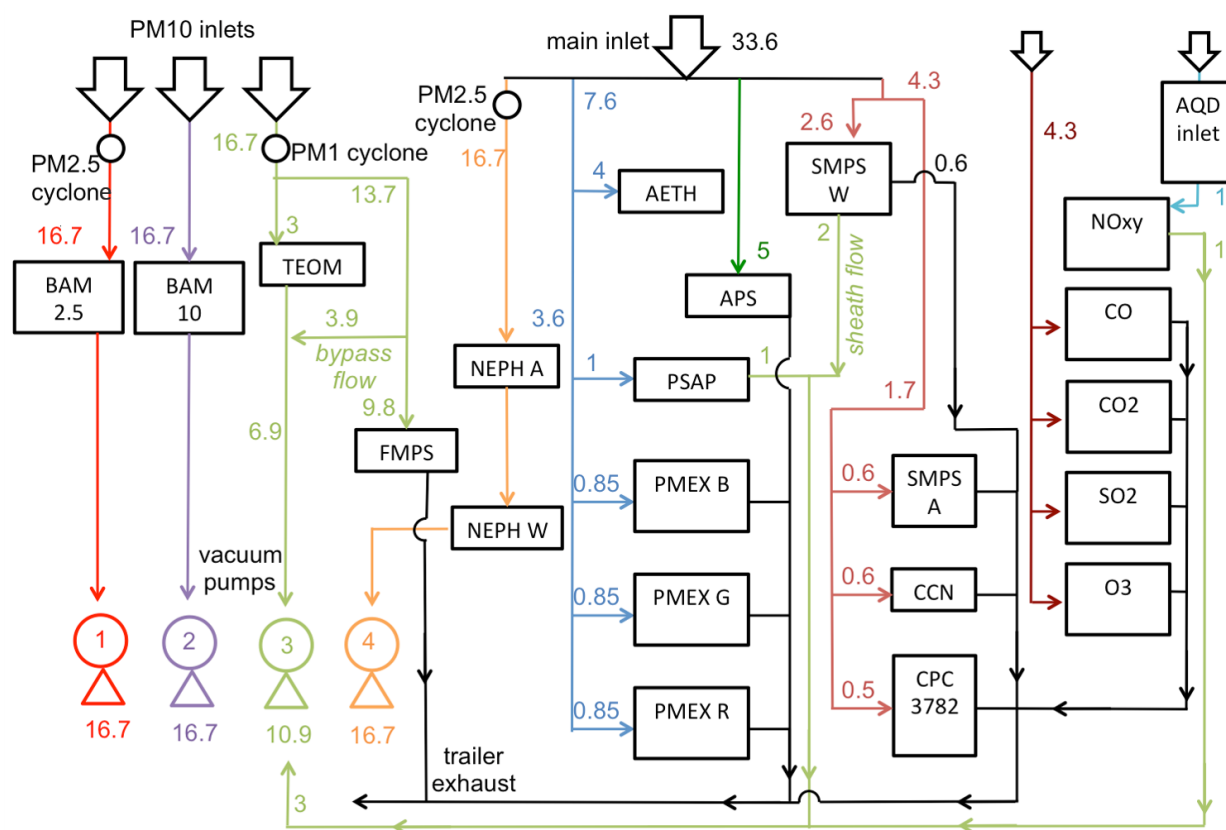


Fig. 1. Schematic of sample flow within COMMIT. Instruments sample ambient (or humidified) air via six separate pathways. Each BAM samples air individually, downstream of PM_{10} size selective inlets (red, purple lines). TEOM and FMPS sample air downstream of a PM_1 sharp cut cyclone (light green line). Gas monitors sample air independently of all other instruments (brown line), with NO_x flow passing through the modified AQD inlet (cyan line). Other instruments from Table 1 sample from the main sampling stack, with NEPH sample air passing through a $PM_{2.5}$ sharp cut cyclone (orange line). All flows are listed, with units in liters per minute ($L \min^{-1}$). Vacuum pumps, labeled 1–4, actively pump air through instruments and outside the laboratory. Instruments not connected to vacuum pumps sample air via internal pumps and exhaust it passively outside the laboratory.

Table 2. Listing of instrument zero-air test lengths and intercomparison tests completed before, during, and after each campaign.

Instrument	Zero-Air Test	Intercomparisons
PMEx	1-hour before/after campaign	NA
AE31	24-hour before/after campaign	Ambient air sampling with PSAP, 1-hour
PSAP	1-hour before/after campaign	Ambient air sampling with AE31, 1-hour
NEPH	1-hour before/after campaign	Ambient air sampling, with/without waterless humidifier bypassed, 24-hours
BAM	24-hour before/after campaign	Ambient air sampling with TEOM, no size-cut, 24-hours
TEOM	24-hour before/after campaign	Ambient air sampling with BAM, no size-cut, 24-hours
APS	1-hour before/after campaign	Atomizer-generated aerosol check, 1-hour
FMPS	1-hour before/after campaign	Atomizer-generated aerosol check, 1-hour
SMPS	1-hour before/after campaign	Ambient air sampling, with/without waterless humidifier bypassed, closed-loop/flow-through sheath flow modes, 5-scans
CCN Counter	1-hour before/after campaign	Atomizer-generated aerosol check, 1-hour
Gas Monitors	Daily/hourly during campaign	NA

storage (30 TB), significant processing power, and various communication interfaces. The virtualized platform allows for the deployment of new or guest instruments without changing any supporting architecture. By using this system, reliability is increased and maintenance requirements are decreased, which allows COMMIT to perform in challenging environments with less manpower. Following a deployment, raw data files are quality-controlled and processed into Network Common Data Format (netCDF) for archiving.

METHODS AND RESULTS

Trace Gas Measurements

COMMIT houses six trace gas analyzers that measure gas concentration (Fig. 1, dark red lines) using a variety of methods including chemiluminescence and infrared absorption. Ambient air passes through a particle filter to remove large particles prior to sampling. All gas monitors are regularly calibrated using a dynamic gas calibrator and predefined spans of a National Institute of Standards and Technology (NIST)-traceable, known gas mixture containing CO₂, CO, SO₂, and NO. The plumbing has been modified to allow seamless switching between calibration and sampling modes using a three-way valve. The zero-air generation system described above is periodically used to challenge the monitors with purified air to test their baseline readings. However, a traceable ozone source is required to calibrate the ozone monitor.

Air Quality Design, Inc. (AQD) upgraded a 42C Chemiluminescence NO-NO₂-NO_x Analyzer in 2011. The upgrade includes a redesigned sampling inlet containing a blue light converter that converts NO₂ to NO in the presence of O₃ at a ~50% conversion rate. Various valves direct sample flow to the blue light converter and to a molybdenum converter (for conversion of NO_x + other nitrogen species [NO_y] to NO), and then the 42C for direct measurement of NO by chemiluminescence (Fig. 1, light blue/light green lines). The modified AQD sampling inlet is located close to the converters to minimize the physical distance between them. The monitor undergoes the same multi-point span calibrations as the other analyzers, with an additional

calibration using n-propyl nitrate (nPN) to qualitatively assess the performance of the NO_y converter.

Ou-Yang *et al.* (2016) analyze several trace gas data sets collected from COMMIT at DAK during 2015 and also make comparisons to observations taken at SL during 2012–2013. They use the data to characterize the age and composition of the air masses of the region and also compare the trace gas ratios from BB-dominated regions and urban pollution dominated regions. Sayer *et al.* (2016) illustrate how peaks in the gas concentration data align well in time with peaks in aerosol loading observed by NASA's Aerosol Robotic Network (AERONET, Holben *et al.*, 1998) of sun photometers.

Optical Measurements

During the DAK and SL campaigns, aerosol loading due to BB was often high enough to cause loss of sensitivity in the optical instruments. For example, aerosol deposition on the filter-based Particle Soot Absorption Photometer (PSAP) would decrease optical transmission of light to below 70% of reference transmission within one hour during poor air quality days, a threshold below which Bond *et al.* (2010) showed that instrument calibrations are no longer valid. The Cavity-Attenuated Phase Shift Monitor (PMEx), an optical extinction monitor, measures the time that light spends inside a sample cell bound by two mirrors. The time decreases as particle concentration increases due to forward scattering of the light by the particles (Petzold *et al.*, 2013), so contamination of the mirrors directly affects the efficiency at which this occurs, particularly when the loss is greater than 1500 Mm⁻¹, and results in periods of missing data. Changing filters and cleaning mirrors frequently using a positive pressure clean room and filtered air helps avoid downtime.

An Aethalometer (AE31, Fig. 1, blue line) measures black carbon concentrations by passing ambient air through a quartz filter and performing continuous optical analysis on the deposited sample at seven wavelengths from 370 to 950 nanometers (nm). The black carbon concentrations at each wavelength are directly proportional to absorption coefficients (σ_a), which are then corrected according to

Arnott *et al.* (2005) to account for multiple scattering effects. Using the corrected AE31 data strengthens the correlation with σ_a derived from PSAP (Fig. 1, blue line), which provides additional absorption information at three wavelengths.

Optical extinction coefficients (σ_e) are measured using three PMEx monitors (Fig. 1, blue lines) operating at different visible wavelengths (Table 1). Due to the design of the instrument, a small amount of filtered, purged air is required inside the chamber to prevent the mirrors from becoming contaminated. This slightly reduces path length and can be corrected in post-mission analyses (Petzold *et al.*, 2013).

Optical scattering measurements are provided at three wavelengths, measured by a pair of NEPHs. Described in detail below, the pair consists of two identical NEPHs, one sampling ambient air (NEPH_A) and one sampling humidified air (NEPH_W), to extract hygroscopic aerosol effects on optical scattering. Instrument intercomparisons are conducted with data from NEPH_A so that RH is similar between absorption, extinction, and scattering coefficient measurements.

Fig. 2 illustrates a closure study with data from DAK during 2015, using measurements interpolated to the blue channel (470 nm). During March 2015, high correlations ($r \geq 0.97$) between σ_e , measured by PMEx, and the sum of σ_a and σ_s , measured by an AE31 and NEPH_A, respectively, indicate that the measurements are consistent between platforms. There is a linear relationship between PMEx extinction vs. AE31 and NEPH_A with a gradient of ~ 0.94 and small intercept, meaning larger values of extinction are estimated by summing AE31 and NEPH_A than are estimated by directly observing extinction using PMEx. Deviation

from a slope of unity could be attributed to the use of a PM_{2.5} cyclone for the NEPH, however in a BB atmosphere, particles larger than PM_{2.5} contribute comparatively less than smaller particles to extinction in the visible and are not expected to be present in large concentrations (during the period from 1–20 March 2015 at DAK, the mean and standard deviation of the PM_{2.5}/PM₁₀ ratio was $89.5\% \pm 8.8\%$). Performing the analysis for the same time frame using PSAP σ_a also gives high correlations (> 0.97), but the linear relationship is weaker (gradient ~ 0.84) than that seen using AE31.

Sayer *et al.* (2016) provide a detailed analysis and comparison between Moderate Resolution Imaging Spectroradiometer (MODIS) Deep Blue aerosol products, COMMIT optical *in-situ* data, and SSA observed by a collocated sun photometer operated by AERONET at DAK. They determined that surface SSA was well correlated with AERONET retrievals of column SSA, but that a low offset (more strongly absorbing aerosols) was present in the *in-situ* COMMIT data, attributed to a combination of discrepancies in aerosol loading throughout the atmospheric column versus at the surface, and potential instrumental/retrieval artifacts.

Microphysical Measurements

In addition to the hygroscopic growth measurements obtained using a paired Scanning Mobility Particle Sizer (SMPS) system, described below, particle mass concentrations are also assessed using two BAMs (filter attenuation-based, Gobeli *et al.*, 2008) and a TEOM (particle mass-based,

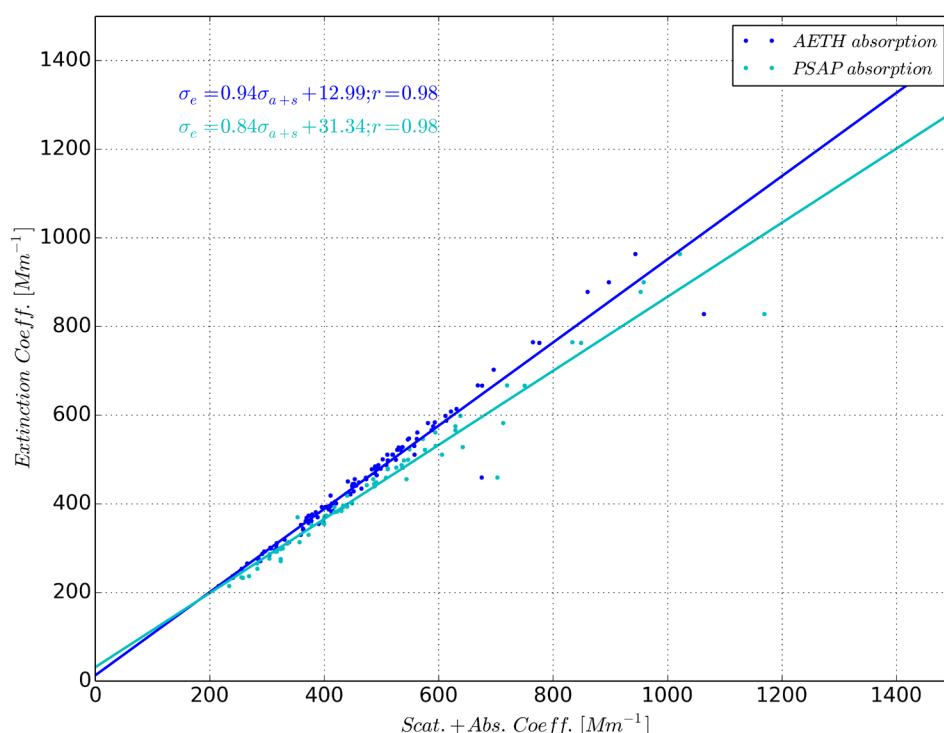


Fig. 2. Optical closure at 470 nm calculated from hourly-averaged data observed during 7-SEAS/BASELInE at DAK from 1–20 March 2015. Blue (cyan) dots assume σ_e by summing σ_s from corrected NEPH_A and absorption σ_a from corrected AE31 (PSAP) data.

Allen *et al.*, 1997). To fully characterize and distinguish between fine ($< \text{PM}_{2.5}$) and coarse ($\text{PM}_{2.5}$ – PM_{10}) aerosol particles, one BAM operates behind a PM_{10} inlet (Fig. 1, BAM10) and another behind both a PM_{10} inlet and a $\text{PM}_{2.5}$ size-cut cyclone (Fig. 1, BAM2.5). The TEOM operates behind a PM_{10} inlet and a PM_1 size-cut cyclone (Fig. 1, light green line).

An Aerodynamic Particle Sizer (APS, Fig. 1, green line) and a Fast Mobility Particle Sizer (FMPS, Fig. 1, light green line) provide additional PSD information to extend that of SMPS and to complement the particle mass information from TEOM and BAMs. APS reports aerodynamic particle diameters, geometric means, and geometric modes; FMPS and SMPS report the same information, but for electrical mobility diameter. All particle sizers were configured to report number concentrations [dN/dlogdp] at identical time intervals to simplify intercomparisons. FMPS operates behind a PM_1 size-cut cyclone along with TEOM to provide high temporal resolution information on PSD of fine-mode particles.

Following Khylstov *et al.* (2005) and Bell *et al.* (2013), SMPS and APS data are post-processed and merged to create a continuous PSD ranging from 20 nm to 20 μm , accounting for differences in measurements of aerodynamic diameter mobility and electrical mobility. This technique shifts the APS PSD to match a power fit of SMPS data in the overlap region (~ 520 nm–900 nm) and provides a visualization of a wide range of ambient aerosol particles that is not commonly observed with any single instrument, particularly when mineral dust and BB aerosols are mixed together in a region.

A Cloud Condensation Nuclei (CCN) counter provides CCN number concentration at various supersaturation ratios (Fig. 1, pink line). These data are further explored by Hsiao *et al.* (2016), who analyzed the diurnal patterns of CCN and determined that fresh BB aerosols were composed mainly of particulate organic matter during the DAK campaign. Calibration of the CCN counter is conducted by sampling atomizer-generated ammonium sulfate particles of a known diameter.

Hygroscopic Measurements and Analysis

COMMIT collects continuous observations of hygroscopic effects on aerosol scattering, PSD, and mean geometric particle diameter. These provide two robust datasets that are unique but correlated, and thus valuable for furthering the understanding of aerosol behavior in high RH environments; they will be of particular interest to studies of BB aerosols in SEA.

A humidification system, similar to the water-based system described by Titos *et al.* (2014), is the critical component for the hygroscopic analysis. The humidifier was developed and tested in the laboratory (Fig. 3(a)). The unit consists of a 30 cm long Gore-Tex tube with a 1.5 cm inner diameter, through which a sample of ambient-RH air passes with minimal particle loss or modification assumed. Stainless steel coils are embedded inside the tube to maintain its structure at high flow rates. A plastic cylinder surrounds the tube and is filled with temperature-controlled distilled water that is

heated and recirculated through a water bath. Compared to a diffusion membrane humidifier, this design allows the desired sample RH to be achieved quickly by adjusting the temperature of the recirculating water. As shown in Fig. 3(b), the humidifier can generate an ambient air sample with a temporally stable RH. Sharp changes of ambient RH are dampened by passage through the humidifier, which ensures consistent measurements of hygroscopicity. By adjusting the humidified air flow and temperature of the water from 2–20 liters per minute (L min^{-1}) and 20–50°C, respectively, a sample RH of anywhere from 35–90% can be maintained, although it is generally maintained at or above 85% for hygroscopic growth studies, a level suggested by Titos *et al.* (2004).

The performance of this system was validated by checking the hygroscopic growth of laboratory-generated 100 nm sodium chloride particles. The critical humidity (the RH at which particles grow rapidly) of the experimental particles was observed at 75.3%, compared to literature values $\sim 75\%$, which confirms the capability of the humidification system. Temperature and RH sensors (PTB210s, Vaisala, Finland) continuously monitor conditions upstream and downstream of the humidifiers to ensure stable performance.

During normal operations, the humidification system is operated with two identical instruments (one sampling ambient air and the other sampling humidified air) to obtain simultaneous measurements at different RH. This setup has benefits compared to operating a single instrument with switched air flows, since uncertainties related to sampling time, instrument response, and disruptions of flow are all avoided by maintaining continuous measurements. However, characterization and calibration of the individual instruments to account for their systematic differences is required prior to data analysis to ensure high quality results.

Hygroscopic enhancement of light scattering coefficients (σ_s) of aerosols is measured with two integrating NEPH instruments operating in series (Fig. 1, orange line). Total scattering and backscattering coefficients at three wavelengths (Table 1) are reported throughout the deployment and corrected for angular nonidealities as described by Anderson and Ogren (1998).

As shown in Fig. 4, ambient air exhausted by NEPH_A passes through the humidification system and is redirected as input for NEPH_W to keep flow conditions identical between instruments. Anderson and Ogren (1998) demonstrated that NEPHs operating in series have no significant particle loss beyond the uncertainty of the instruments. The original NEPH blowers were removed and replaced with an external pump to control the fixed flow rate at 16.7 L min^{-1} required by the upstream $\text{PM}_{2.5}$ size-cut cyclone. Other cyclones or selective inlets may be placed upstream to further categorize the sample, particularly if particle diameter/human health is of interest.

Before and after each campaign, the paired NEPH system is tested and calibrated rigorously. Most commonly, users perform a gaseous calibration using CO_2 , which has a well-known σ_s , although other gases have been proposed (Anderson and Ogren 1998; Abu-Rahman *et al.* 2006). Another method is to use white (non light-absorbing)

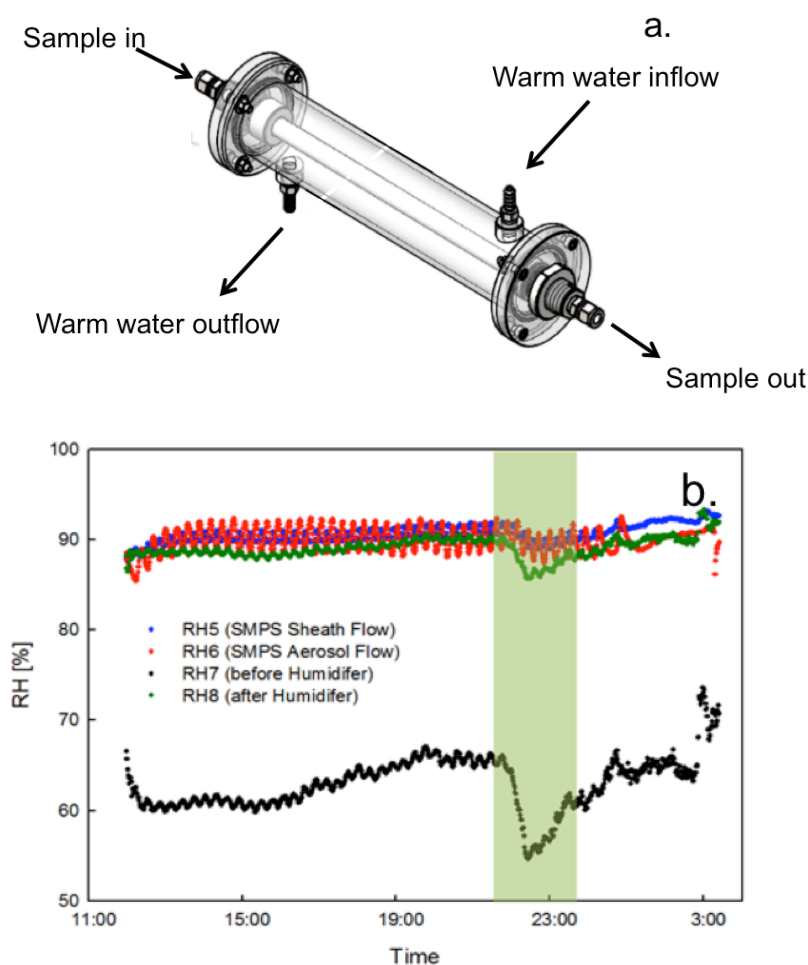


Fig. 3. a: Diagram showing the design of the humidifier for the tandem NEPH and SMPS hygroscopic systems. Air flows through a central tube made of Gore-Tex that is surrounded by a cylinder with recirculating warm water. b: Time series of 16 hours of RH data from various sensors mounted through the SMPS_w system, upstream and downstream of the humidification system, during April 2015.

aerosol particles to characterize the NEPH's performance at higher σ_s than is normally observable for particle-free, gaseous air (Abu-Rahman *et al.*, 2006). In addition to calibrating the NEPHs with filtered air and CO₂, the effects of the humidification system on the measurements are also characterized. First, scattering measurements between NEPH_A and NEPH_w are compared with the humidifier removed from the sampling line to determine the baseline performance of each instrument. Before and after the DAK campaign, there was good agreement in slope (1.03–1.12 pre-campaign, 0.98–1.03 post-campaign) and correlation ($r = 0.97$ – 0.98 pre-campaign, 0.85 – 0.86 post-campaign) at all wavelengths between instruments sampling ambient air for 24 hours. As an alternate test, the humidifier in front of NEPH_w is replaced, but with the flow of water stopped. In this sense, the degree of particle loss across the Gore-tex tube, which is assumed to be minimal, is determined without the additional effect of hygroscopic growth due to the warm water. Titos *et al.* (2014) conducted similar tests of their humidification system, during periods when the reference NEPH closely matched the humidity of the RH-modified NEPH. Completion of these tests before and after each

campaign provides important baselines and flow calibrations, which are taken into account during subsequent analyses.

Hygroscopic effects on aerosol microphysical properties are assessed using a tandem SMPS system with a humidifier like that used for the NEPH system (Fig. 1, pink lines). Unlike the NEPHs, however, the humidified SMPS (SMPS_w) and ambient SMPS (SMPS_A) run in parallel. Each SMPS consists of an X-ray neutralizer (TSI3087) to obtain Boltzmann charge equilibrium, a differential mobility analyzer (DMA3081) to classify the aerosols by size, and a condensation particle counter (CPC3787) to determine number concentrations (Table 1). The sheath and aerosol flow rates are set at 2.0 and 0.6 L min⁻¹, respectively, and they were specifically chosen to extend the PSD range up to 1000 nm.

SMPS_A samples ambient air, and its sheath and excess flows are recirculated between it and the classifier (Fig. 4) in a closed-loop system. SMPS_w samples air downstream of a humidifier, and sheath flow passing through the DMA is pulled by a mass flow controller from the humidified sample stream in a “flow-through” mode. This design eliminates a potential imbalance in RH between the humidified aerosol

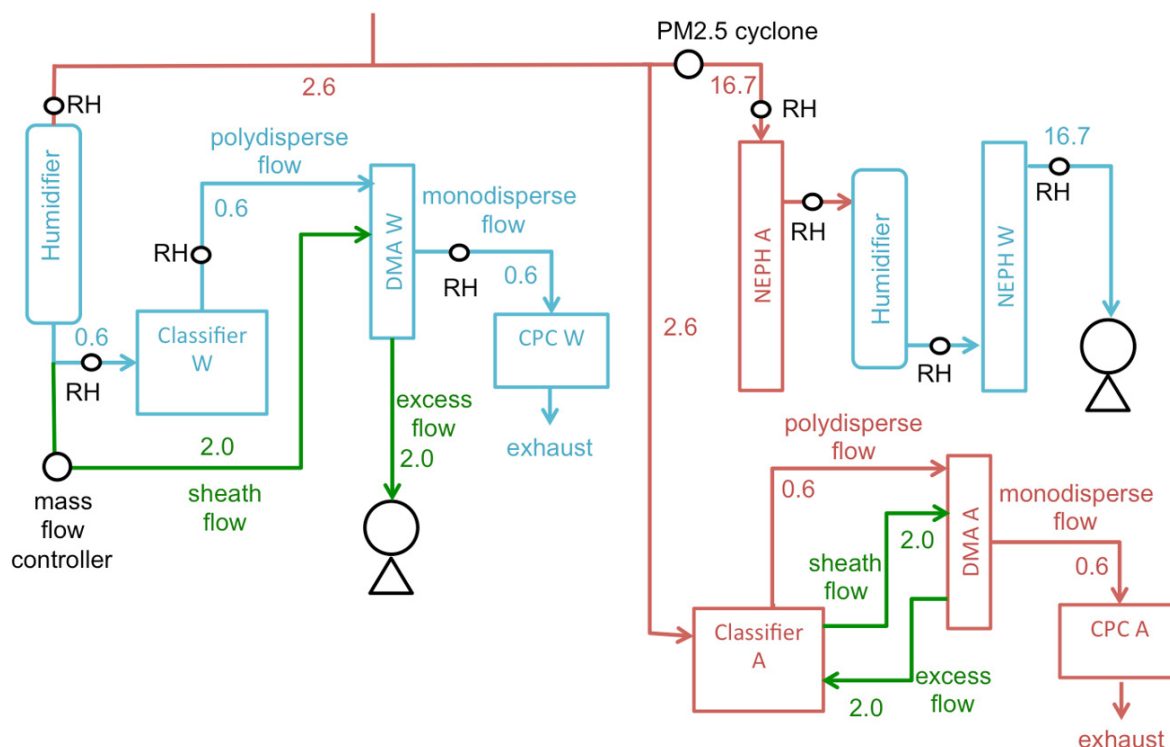


Fig. 4. Simplified schematic of the sample flow within the humidified/ambient SMPS and NEPH systems. Red arrows indicate ambient/non-humidified air sampled by SMPS_A and NEPH_A. Blue arrows indicate humidified air sampled by SMPS_W and NEPH_W. Note difference in plumbing (green arrows) between SMPS_W and SMPS_A sheath flows, which is necessary in order to maintain a humidified sheath flow for SMPS_W. Flows along the individual lines are listed in L min⁻¹.

flow from the classifier and the otherwise unhumidified sheath/excess flow (comparable to studies by Massling *et al.*, 2007). Lab testing indicates that the difference in humidified sheath and humidified sample flows can be reduced to within $\pm 1\%$. The same sensors used for the humidified NEPH system monitor RH throughout the SMPS system. Likewise, RH is fully adjustable based on the temperature of the associated water bath, although flow rates and temperature ranges are adjusted to meet the requirements of the SMPS flow.

Extensive inter-comparisons are conducted before and after the campaign to assess characteristics of the paired SMPS system (*cf.* Table 2). Traditionally, inorganic salt particles like ammonium sulfate (Svenningsson *et al.*, 2006; Mikhailov *et al.*, 2009; Suda and Petters, 2013), a calibration dust standard (Denhean *et al.*, 2014), or polystyrene latex (PSL) particles with known diameters (Hennig *et al.*, 2005) are used for calibration and hygroscopic analysis of particle sizers. In this operation, the performance and effect of the humidification system is characterized using a series of different plumbing schemes. First, with the humidifier bypassed, the baseline measurements of each instrument operating under a closed-loop sheath flow mode are recorded. Next, SMPS_W is switched to “flow-through” mode with the humidifier bypassed. Finally, the humidifier is added back into the SMPS_W sampling line, without water flow, to determine the combined effect of the “flow-through” sheath modification and particle loss across the humidifier. Suda and Petters (2013) calibrate their tandem DMAs in a similar

way, characterizing flow and voltage differences before further analysis of their data.

A calibration was conducted at the end of the DAK campaign in April 2015 (Fig. 5). The results showed that the number concentration was consistently greater in SMPS_A compared to SMPS_W even during calibration tests, with SMPS_W reporting concentrations around 80% of those observed by SMPS_A at the middle of the observable PSD. This result was also observed prior to the start of the campaign, with little change in overall concentrations between instruments during pre- and post-mission calibrations. The differences may arise from counting uncertainties or flow rate differences in the CPCs for particles at low concentrations. To make further comparisons for this analysis, the number-weighted PSDs for each instrument are normalized by the corresponding total concentrations. The normalized PSD eliminates the concentration discrepancy and allows for the direct comparison of the sizing changes (*i.e.*, particle growth) due to the humidification process.

For the calibration test where SMPS_W operated in closed-loop mode with no humidifier (Fig. 5(A)), the mode particle diameter of the PSD for SMPS_W occurred at 113.5 nm, whereas it was 109.4 nm for SMPS_A. Using “flow-through” mode (Fig. 5(B)), the mode occurred at 145.9 nm for SMPS_A and 151.2 nm for SMPS_W. After adding the waterless humidifier back in line (Fig. 5(C)), the mode occurred at 145.9 nm for SMPS_A and 135.8 nm for SMPS_W. For each calibration test, the mode particle diameter were within one or two bins of each other ($< 2\%$ of the full 114

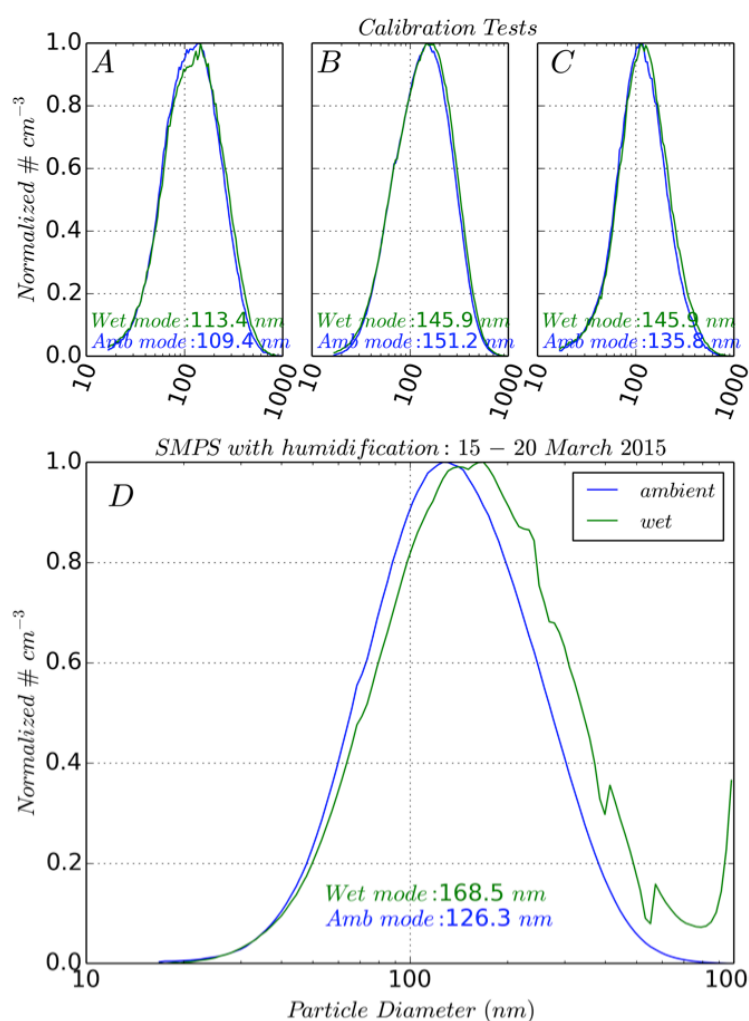


Fig. 5. A: Comparison of number concentration between SMPS_W (blue) and SMPS_A (green), with SMPS_W operating in closed-loop mode with humidification bypassed (calibration test), for 5 consecutive scans. Each PSD is normalized as described in the text. Mode particle diameters for each PSD are displayed for reference. B: Same as A, but with SMPS_W in flow-through mode. C: Same as B, but with the humidifier in line (no water). D: Normalized PSDs averaged over all times during normal operations from 15–20 March 2015, whenever SMPS_W RH > 85% and SMPS_A RH < 40%.

bin range of the SMPS), which reveals that the PSDs were relatively stable between SMPS_A and SMPS_W within each of the various calibration tests. The difference in particle modes between tests is due to the fact that they were conducted over several hours and air masses changed between sampling periods. Therefore, it appears that the presence of the humidifier does not substantially modify the sample flow.

Based on data collected during several days at DAK, the results demonstrate that hygroscopic growth was successfully obtained using the setup described above for the NEPH and SMPS systems. Fig. 5(D) shows the averaged, normalized PSDs for SMPS_W and SMPS_A from 15–20 March 2015 at DAK. For this study, all times when SMPS_W RH was greater than 85% and when SMPS_A RH was less than 40% were considered. After normalization of the PSDs, the SMPS_W PSD appears noticeably shifted rightward, with the mode particle diameter for SMPS_W at 168.5 nm compared to 126.3 nm for SMPS_A, a difference of eight bins (7.0% of the full 114 bin range of the SMPS).

Scattering enhancement, f [RH], describes the increase in optical scattering of aerosols due to their hygroscopic growth. It is normally reported at 85% RH and given by:

$$f[RH] = \frac{\sigma_{s\ wet}}{\sigma_{s\ dry}} = a(100 - RH)^{-\gamma} \quad (1)$$

where $\sigma_{s\ wet}$ ($\sigma_{s\ dry}$) describes optical scattering at high (low) RH, a describes the enhancement as RH approaches 100%, and γ describes the magnitude of the enhancement. The NEPHs at DAK demonstrated that f [RH = 85%] ranged from 1.20 for the blue wavelength to 1.28 for the red wavelength (Fig. 6(A)). The degree of scattering enhancement, γ , is related to wavelength, with longer wavelengths exhibiting higher γ . Previous reviews have shown a wide range in f [RH = 85%], from 1.1–2.2 for BB aerosols (Reid *et al.*, 2005) and from 1.2–3.5 for non-BB aerosols (Titos *et al.*, 2014). This variability is attributed to differences in aerosol type,

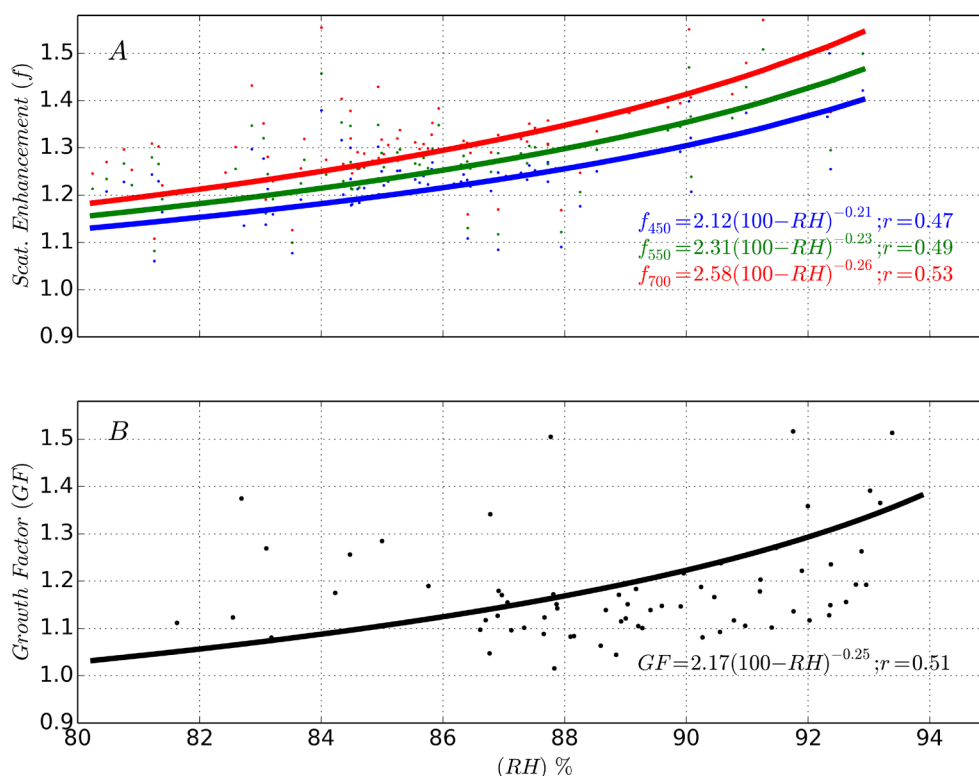


Fig. 6. A: f [RH] vs. RH curves calculated from daily-averaged, corrected NEPH_A and NEPH_W data from DAK from 15 – 20 March 2015 at three wavelengths (450 nm, 550 nm, 700 nm), demonstrating scattering enhancement at high RH during the period. Only data when humidified RH is > 80% (wet) and ambient RH is < 40% (dry) are included. Humidified (ambient) RH is the average of RH observed by sensors located upstream and downstream of NEPH_W (NEPH_A), downstream (upstream) of the humidifier. B: Same as upper panel, but for GF [RH] vs. RH curves calculated using daily-averaged, SMPS geometric mean data.

location, season, age, and hysteresis effects. Particle growth factor, GF [RH], is an analog of f [RH] and describes the increase in mean geometric particle diameter for humidified aerosols. From the observations of the SMPS at DAK, the value of GF [RH = 85%] was 1.10 with $\gamma = 0.25$ (Fig. 6(B)), which is consistent with the small f [RH = 85%] observed.

CONCLUSIONS

7-SEAS/BASELInE marked an important deployment of the COMMIT mobile laboratory into a BB-rich aerosol environment, complementing other 7-SEAS observations from 2012–2013. After analysis of various measurements, we conclude that our SOPs are conducive to continuous, quality controlled data streams of value to the aerosol community. Our extensive observations of anthropogenic and naturally occurring trace gases and optical/microphysical properties of aerosols (particularly BB aerosols) may be applied to derive further information about the air quality of a particular region. Several related studies demonstrated that the calibrated trace gas measurements have the potential to characterize the age and composition of observed aerosols. Our closure analysis validated the scattering/absorption/extinction measurements and suggests that they can be reliably used to pursue studies on aerosol effects on SSA and the radiation budget. Finally, microphysical measurements of

particle size, mass, and concentration have obvious implications to human health and longevity.

The key finding of this analysis stems from the hygroscopic growth setup for the paired NEPH and SMPS instruments. The system is well characterized, and both hygroscopic growth and scattering enhancement were observed during the latest campaign in DAK. Calibration of the systems before and after operations ensures that the humidification itself does not introduce major artifacts into the data streams. Hygroscopic measurements will help characterize aerosol behavior in high RH environments and is expected to play a major role in the analysis of BB and aerosols in SEA since they have not been extensively studied in the literature. In combination with remote sensing data on internal cloud structure obtained with ACHIEVE, COMMIT hygroscopic monitoring will advance the understanding of aerosol-cloud interactions in a region where those effects are poorly known.

Future deployments will continue to emphasize wherever BB aerosols play a major role in pollution and climate forcing. However, focus may shift to megacity regions, where urban pollution and smog outweigh the effects of BB. Such studies would provide an interesting contrast to the recent studies of SEA, and have been preliminary pursued in campaigns such as Deriving Information on Surface Conditions from Column and Vertically Resolved

Observations Relevant to Air Quality (Discover-AQ), when COMMIT collected several months of observations near GSFC in Maryland.

More extensive analysis of hygroscopic growth is currently in progress. In this study, systematic differences were observed in the measurements between the CPCs that comprise the SMPS systems. For this particular analysis, number-weighted PSDs from SMPS were normalized by total concentration and used to compare the size changes between humidified and ambient particles to reduce the effect of the discrepancy. Through a complete examination instrument performance and parameters, including the comparison of the raw particle counts of the PSDs from the CPCs, we hope to determine the source and resolve the concentration discrepancy before the next field deployment, and therefore eliminate the need for normalization of the SMPS data.

Additionally, a logic-controlled feedback loop is being integrated into the NEPH/SMPS humidification system. This will allow the recirculated water to not only be heated, but to be chilled as well. This upgrade will ensure a more stable RH of the humidified instrument flow, and one that is resistant to transient changes in ambient air temperature.

Finally, measurements of dried particles and volatile organic compounds would complement the suite of COMMIT observations, extending the ability to access hygroscopic effects on aerosols and air quality. After the current humidification system is upgraded, tested, and completed, focus will shift to these types of measurements and the hardware required to obtain them.

Data are already available upon request through direct communications with the NASA SMARTLabs team. However, a new web interface is in development, and it will allow community access to various levels of quality-controlled/post-processed datasets and visualizations from current and past field campaigns.

ACKNOWLEDGMENTS

We acknowledge the continuous support of SMARTLabs by the NASA Radiation Sciences Program managed by Dr. Hal B. Maring. We thank staff at Silpakorn University, Chiang Mai University, and the DAK meteorological station in Thailand, and staff at National Central University in Taiwan for their collaboration and support during various international field campaigns. Finally we recognize the Vietnam Ministry of Science and Technology and Vietnam Academy of Science and Technology (project DTDL.3-2011-NCCB and project VT/CB-02/14-15 under Vietnam Program of Space Technology) and the SL meteorological station in Vietnam.

REFERENCES

- Abu-Rahmah, A., Arnott, W.P. and Moosmüller, H. (2006). Integrating nephelometer with a low truncation angle and an extended calibration scheme. *Meas. Sci. Technol.* 17: 1723–1732.
- Allen, G., Sioutas, C., Koutrakis, P., Reiss, R., Lurmann, F.W. and Roberts, P.T. (1997). Evaluation of the TEOM® method for measurement of ambient particulate mass in urban areas. *J. Air Waste Manage. Assoc.* 47: 682–689.
- Anderson, T.L. and Ogren, A. (1998). Determining aerosol radiative properties using the TSI 3563 integrating nephelometer. *Aerosol Sci. Technol.* 29: 57–69.
- Andreae, M.O. and Merlet, P. (2001). Emission of trace gases and aerosols from biomass burning. *Global Biogeochem. Cycles* 15: 955–966.
- Arnott, W.P., Hamasha, K., Moosmüller, H., Sheridan, P.J. and Ogren, J.A. (2005). Towards aerosol light-absorption measurements with a 7-wavelength aethalometer: Evaluation with a photoacoustic instrument and 3-wavelength nephelometer. *Aerosol Sci. Technol.* 39: 17–29.
- Bell, S.W., Hansell, R.A., Chow, J.C., Tsay, S.C., Hsu, N.C., Lin, N.H., Wang, S.H., Ji, Q., Li, C., Watson, J.G. and Khlystov, A. (2013). Constraining aerosol optical models using ground-based, collocated particle size and mass measurements in variable air mass regimes during the 7-SEAS/Dongsha experiment. *Atmos. Environ.* 78: 163–173.
- Bond, T.C., Anderson, T.L. and Campbell, D. (2010). Calibration and intercomparison of filter-based measurements of visible light absorption by aerosols. *Aerosol Sci. Technol.* 30: 582–600.
- Booth, B.B.B., Dunstone, N.J., Halloran, P.R., Andrews, T. and Bellouin, N. (2012). Aerosols implicated as a prime driver of twentieth-century North Atlantic climate variability. *Nature* 484: 228–232.
- Brauer, M., Amann, M., Burnett, R.T., Cohen, A., Dentener, F., Ezzati, M., Henderson, S.B., Krzyzanowski, M., Martin, R.V., Van Dingenen, R., van Donkelaar, A. and Thurston, G.D. (2012). Exposure assessment for estimation of the global burden of disease attributable to outdoor air pollution. *Environ. Sci. Technol.* 46: 652–660.
- Brook, R.D., Rajagopalan, S., Pope, C.A., 3rd, Brook, J.R., Bhatnagar, A., Diez-Roux, A.V., Holguin, F., Hong, Y., Luepker, R.V., Mittleman, M.A., Peters, A., Siscovick, D., Smith, S.C., Jr., Whitsel, L., Kaufman, J.D., American Heart Association Council on Epidemiology and Prevention, Council on the Kidney in Cardiovascular Disease, and Council on Nutrition, Physical Activity and Metabolism (2010). Particulate matter air pollution and cardiovascular disease: An update to the scientific statement from the American Heart Association. *Circulation* 121: 2331–2378.
- Chan, C.Y., Chan, L.Y., Harris, J.M., Oltmans, S.J., Blake, D.R., Qin, Y., Zheng, Y.G. and Zheng, X.D. (2003). Characteristics of biomass burning emission sources, transport, and chemical speciation in enhanced springtime tropospheric ozone profile over Hong Kong. *J. Geophys. Res.* 108: 4015.
- Chantara, S., Sillapapiromsuk, S. and Wiriya, W. (2012). Atmospheric pollutants in Chiang Mai (Thailand) over a five-year period (2005–2009), their possible sources and relation to air mass movement. *Atmos. Environ.* 60: 88–98.
- Chuesaard, T., Chetianukornkul, T., Kameda, T., Hayakawa,

- K. and Toriba, A. (2014). Influence of biomass burning on the levels of atmospheric polycyclic aromatic hydrocarbons and their nitro derivatives in Chiang Mai, Thailand. *Aerosol Air Qual. Res.* 14: 1247–1257.
- Eck, T.F., Holben, B.N., Reid, J.S., Dubovik, O., Smirnov, A., O'Neill, N.T., Slutsker, I. and Kinne, S. (1999). Wavelength dependence of the optical depth of biomass burning, urban, and desert dust aerosols. *J. Geophys. Res.* 64: 31333–31349.
- Engelhart, G.J., Hennigan C.J., Miracolo, M.A., Robinson, A.L. and Pandis, S.N. (2012). Cloud condensation nuclei activity of fresh primary and aged biomass burning aerosol. *Atmos. Chem. Phys.* 12: 7285–7293.
- Gautam, R., Hsu, N.C., Eck, T.F., Holben, B.N., Janjai, S., Jantarach, T., Tsay, S.C. and Lau, W.K. (2013). Characterization of aerosols over the Indochina peninsula from satellite-surface observations during biomass burning pre-monsoon season. *Atmos. Environ.* 78: 51–59.
- Gobeli, D., Schloesser, H. and Pottberg, T. (2008). Met One Instruments BAM-1020 BetaAttenuation Mass monitor US-EPA PM_{2.5} Federal Equivalent Method field test results, Paper #2008-A-485-AWMA.
- Hennig, T., Massling, A., Brechtel, F.J. and Wiedensohler, A. (2005). A tandem DMA for highly temperature-stabilized hygroscopic particle growth measurements between 90% and 98% relative humidity. *J. Aerosol Sci.* 36: 1210–1223.
- Hervo, M., Sellegri, K., Pichon, J.M., Roger, J.C. and Laj, P. (2014). Lon term measurements of optical properties and their hygroscopic enhancement. *Atmos. Chem. Phys.* 14: 27731–27767.
- Holben, B.N., Eck, T.F., Slutsker, I., Tanré, D., Buis, J.P., Setzer, A., Vermote, E., Reagan, J.A., Kaufman, Y.J., Nakajima, T., Lavenue, F., Jankowiak, I. and Smirnov, A. (1998). AERONET: A federated instrument network and data archive for aerosol characterization. *Remote Sens. Environ.* 66: 1–16.
- Hsiao, T.C., Ye, W.C., Wang, S.H., Tsay, S.C., Chen, W.N., Lin, N.H., Lee, C.T., Hung, H.M., Chuang, M.T. and Chantara, S. (2016). Investigation of the CCN activity, BC and UVBC mass concentrations of biomass burning aerosols during the 2013 BASELInE campaign. *Aerosol Air Qual. Res.* 16: 2742–2756.
- Hu, D., Qiao, L., Chen, J., Ye, X., Yang, X., Cheng, T. and Fang W. (2010). Hygroscopicity of inorganic aerosols: size and relative humidity effects on the growth factor. *Aerosol Air Qual. Res.* 10: 255–264.
- Huang, K., Fu, J.S., Hsu, N.C., Gao, Y., Dong, X., Tsay, S.C. and Lam, Y.F. (2013). Impact assessment of biomass burning on air quality in Southeast and East Asia during BASE-ASIA. *Atmos. Environ.* 78: 291–302.
- Khylstov, A., Stanier, C.O., Takahama, S. and Pandis, S.N. (2005). Water content of ambient aerosol during the Pittsburgh Air Quality Study. *J. Geophys. Res.* 110: D07S10.
- Kondo, Y., Matsui, H., Moteki, N., Sahu, L., Takegawa, N., Kajino, M., Zhao, Y., Cubison, M.J., Jimenez, J.L., Vay, S., Diskin, G.S., Anderson, B., Wisthaler, A., Mikoviny, T., Fuelberg, H.E., Blake, D.R., Huey, G., Weinheimer, A.J., Knapp, D.J. and Brune, W.H. (2011). Emissions of black carbon, organic, and inorganic aerosols from biomass burning in North America and Asia in 2008. *J. Geophys. Res.* 116: D08204.
- Kristensson, A., Rissler, J., Löndahl, J., Johansson, C. and Swietlicki E. (2013). Size-Resolved respiratory tract deposition of sub-micrometer aerosol particles in a residential area with wintertime wood combustion. *Aerosol Air Qual. Res.* 13: 24–35.
- Lance, S., Nenes, A., Medina, J. and Smith, J.N. (2006). Mapping the operation of the DMT continuous flow CCN counter. *Aerosol Sci. Technol.* 40: 242–254.
- Lelieveld, J., Evans, J.S., Fnais, M., Giannadaki, D. and Pozzer, A. (2015). The contribution of outdoor air pollution sources to premature mortality on a global scale. *Nature* 525: 367–371.
- Lin, C.Y., Hsu, H.M., Lee, Y.H., Kuo, C.H., Sheng, Y.F. and Chu, D.A. (2009). A new transport mechanism of biomass burning from Indochina as identified by modeling studies. *Atmos. Chem. Phys.* 9: 7901–7911.
- Lin, C.Y., Zhao, C., Liu, X., Lin, N.H. and Chen W.N. (2014). Modeling of long-range transport of Southeast Asia biomass-burning aerosols to Taiwan and their radiative forcings over East Asia. *Tellus Ser. B* 66: 23733.
- Lin, N.H., Sayer, A.M., Wang, S.H., Loftus, A.M., Hsiao, T.C., Sheu, G.R., Hsu, N.C., Tsay, S.C. and Chantara, S. (2014). Interactions between biomass-burning aerosols and clouds over Southeast Asia: Current status, challenges, and perspectives. *Environ. Pollut.* 195: 292–307.
- Lin, N.-H., Tsay, S.C., Maring, H.B., Yen, M.C., Sheu, G.R., Wang, S.H., Chi, K.H., Chuang, M.T., OuYang, C.F., Fu, J.S., Reid, J.S., Lee, C.T., Wang, L.C., Wang, J.L., Hsu, C.N., Sayer, A.M., Holben, B.N., Chu, Y.C., Nguyen, X.A., Sopajaree, K., Chen, S.J., Cheng, M.T., Tsuang, B.J., Tsai, C.J., Peng, C.M., Schnell, R.C., Conway, T., Chang, C.T., Lin, K.S., Tsai, Y.I., Lee, W.J., Chang, S.C., Liu, J.J., Chiang, W.L., Huang, S.J., Lin, T.H. and Liu, G.R. (2013). An overview of regional experiments on biomass burning aerosols and related pollutants in Southeast Asia: From BASE-ASIA and the Dongsha experiment to 7-SEAS. *Atmos. Environ.* 78: 1–19.
- Loftus, A.M., Tsay, S.C., Pantina, P., Nguyen, C., Gabriel, P.M., Nguyen, X.A., Sayer, A.M., Tao, W.K. and Matsui, T. (2016). Coupled aerosol-cloud systems over Northern Vietnam during 7-SEAS/BASELInE: A radar and modeling perspective. *Aerosol Air Qual. Res.* 16: 2768–2785.
- Massling, A., Leinert, S., Wiedensohler, A. and Covert, D. (2007). Hygroscopic growth of sub-micrometer and one-micrometer aerosol particles measured during ACE-Asia. *Atmos. Chem. Phys.* 7: 3249–3259.
- Mikhailov, E., Vlasenko, S., Martin, S.T., Koop, T. and Poschl, U. (2009). Amorphous and crystalline aerosol particles interacting with water vapor: conceptual framework and experimental evidence for restructuring, phase transition and kinetic limitation. *Atmos. Chem. Phys.* 9: 9491–9522.

- Orr, C., Hurd, F.K. and Hendrix, W.P. (1958). The behavior of condensation nuclei under changing humidities. *J. Meteorol.* 15: 240–242.
- Ou-Yang, C.F., Tsay, S.C., Wang, S.H., Pantina, P., Li, C., Kuo, F., Nguyen, A.X. and Lin, N.H. (2016). Influence of springtime biomass burning on the characteristics of gaseous air pollutants in Southeast Asia. *Aerosol Air Qual. Res.*, in Preparation.
- Petzold, A., Onasch, T., Kebabian, P. and Freedman, A. (2013). Intercomparison of a Cavity Attenuated Phase Shift-based extinction monitor (CAPS PMex) with an integrating nephelometer and a filter-based absorption monitor. *Atmos. Meas. Tech.* 6: 1141–1151.
- Reid, J.S., Eck, T.F., Christopher, S.A., Koppmann, R., Dubovik, O., Eleuterio, D.P., Holben, B.N., Reid, E.A. and Zhang, J. (2005). A review of biomass burning emissions part III: Intensive optical properties of biomass burning particles. *Atmos. Chem. Phys.* 5: 827–849.
- Rissler, J., Vestin, A., Swietlicki, E., Fisch, G., Zhou, J., Artaxo, P. and Andreae, M.O. (2006). Size distribution and hygroscopic properties of aerosol particles from dry-season biomass burning in Amazonia. *Atmos. Chem. Phys.* 6: 471–491.
- Rutter, A.P., Shakya, K.M., Schauer, J.J. and Griffin, R.J. (2012). Oxidation of gaseous elemental mercury in the presence of secondary organic aerosols. *Atmos. Environ.* 59: 86–92.
- Sayer, A.M., Hsu, N.C., Hsiao, T.C., Pantina, P., Kuo, F., Ou-Yang, C.F., Holben, B.N., Janjai, S., Chantara, S., Wang, S.H., Loftus, A.M., Lin, N.H. and Tsay, S.C. (2016). In-situ and remotely-sensed observations of biomass burning aerosols at Doi Ang Khang, Thailand during 7-SEAS/BASELInE 2015. *Aerosol Air Qual. Res.* 16: 2786–2801.
- Suda, S.R. and Petters, M.D. (2013). Accurate determination of aerosol activity coefficients at relative humidities up to 99% using the hygroscopicity tandem differential mobility analyzer technique. *Aerosol Sci. Technol.* 47: 991–1000.
- Svenningsson, B., Rissler, J., Swietlicki, E., Mircea, M., Bilde, M., Facchini, M.C., Decesari, S., Fuzzi, S., Zhou, J., Mønster, J. and Rosenørn, T. (2006). Hygroscopic growth and critical supersaturations for mixed aerosol particles of inorganic and organic compounds of atmospheric relevance. *Atmos. Chem. Phys.* 6: 1937–1952.
- Tao, J.C., Zhao, C.S., Ma, N. and Liu, P.F. (2014). The impact of aerosol hygroscopic growth on the single-scattering albedo and its application on the NO₂ photolysis rate coefficient. *Atmos. Chem. Phys.* 14: 12055–12067.
- Titos, G., Lyamani, H., Cazorla, A., Sorribas, M., Foyo-Moreno, I., Wiedensohler, A. and Alados-Arboledas, L. (2014). Study of the relative humidity dependence of aerosol light-scattering in Southern Spain. *Tellus Ser. B* 66: 24536.
- Tsai, Y.I., Sopajaree, K., Chotruksa, A., Wu, H.C. and Kuo, S.C. (2013). Source indicators of biomass burning associated with inorganic salts and carboxylates in dry season ambient aerosol in Chiang Mai Basin, Thailand, *Atmos. Environ.* 78: 93–104.
- Tsay, S.C., Maring, H.B., Lin, N.H., Buntoung, S., Chantara, S., Chuang, H.C., Gabriel, P.M., Goodloe, C.S., Holben, B.N., Hsiao, T.C., Hsu, N.C., Janjai, S., Lau, W.K.M., Lee, C.T., Lee, J., Loftus, A.M., Nguyen, A.X., Nguyen, C.M., Pani, S.K., Pantina, P., Sayer, A.M., Tao, W.K., Wang, S.H., Welton, E.J., Wiriya, W. and Yen, M.C. (2016). Satellite-surface perspectives of air quality and aerosol-cloud effects on the environment: An overview of 7-SEAS/BASELInE. *Aerosol Air Qual. Res.* 16: 2581–2602.
- Tsay, S.C., Hsu, N.C., Lau, W.K.M., Li, C., Gabriel, P.M., Ji, Q., Holben, B.N., Judd Welton, E., Nguyen, A.X., Janjai, S., Lin, N.-H., Reid, J.S., Boonjawat, J., Howell, S.G., Huebert, B.J., Fu, J.S., Hansell, R.A., Sayer, A.M., Gautam, R., Wang, S.-H., Goodloe, C.S., Miko, L.R., Shu, P.K., Loftus, A.M., Huang, J., Kim, J.Y., Jeong, M.J. and Pantina, P. (2013). From BASE-ASIA toward 7-SEAS: A satellite-surface perspective of biomass-burning aerosols and clouds in Southeast Asia. *Atmos. Environ.* 78: 20–34.
- Wang, S.H., Welton, E.J., Holben, B.N., Tsay, S.C., Lin, N.H., Giles, D., Stewart, S.A., Janjai, S., Nguyen, X.A., Hsiao, T.C., Chen, W.N., Lin, T.H., Buntoung, S., Chantara, S. and Wiriya, W. (2015). Vertical distribution and columnar optical properties of springtime biomass-burning aerosols over Northern Indochina during 2014 7-SEAS campaign. *Aerosol Air Qual. Res.* 15: 2037–2050.
- Yen, M.C., Peng, C.M., Chen, T.C., Chen, C.S., Lin, N.H., Tzeng, R.Y., Lee, Y.A. and Lin, C.C. (2013). Climate and weather characteristics in association with the active fires in northern Southeast Asia and spring air pollution in Taiwan during 2010 7-SEAS/Dongsha Experiment. *Atmos. Environ.* 78: 35–50.

Received for review, November 18, 2015

Revised, January 14, 2016

Accepted, January 25, 2016